Large-Scale Modeling of Defects in Advanced Oxides: Oxygen Vacancies in $BaZrO_3$ Crystals

Marco Arrigoni, Eugene A. Kotomin, and Joachim Maier

Abstract Quantum mechanical simulations have proved to be an accurate tool in the description and characterization of point defects which can substantially alter the physical and chemical properties of oxides and their applications, e.g. in fuel cells and permeation membranes. Accurate simulations should take into account both the defect energetics in the real material and the thermodynamic effects at finite temperatures. We studied and compared here the structural, electronic and thermodynamic properties of the neutral ($v_O^{\times}$) and the positively doubly charged ($v_O^{\bullet\bullet}$) oxygen vacancies in bulk $BaZrO_3$; particular emphasis was given in the evaluation of the contribution of lattice vibrations on the defect thermodynamic properties. The large-scale computer calculations were performed within the linear combination of atomic orbitals (LCAO) approach and the hybrid of Hartree-Fock method and density functional theory (HF-DFT). It is shown that phonons contribute significantly to the formation energy of the charged oxygen vacancy at high temperatures ($\sim$ 1 eV at 1000 K), due to the large lattice distortion brought by this defect and thus their neglect would lead to a considerable error.

1 Introduction

Perovskite oxides comprise a broad family of technologically important materials, which display a wide range of functional properties, such as ferroelectricity, magnetism, their combination (multiferroics), piezoelectricity, high-temperature superconductivity, mixed ionic-electronic conductivity and electro-optic effects [1–3]. This family of compounds can be described by the ABO_3 formula, where A and B are two cations occupying dodecahedral interstices and oxygen octahedra

M. Arrigoni (✉) • J. Maier
Max Planck Institute for Solid State Research, Heisenbergstraße 1, 70569 Stuttgart, Germany
e-mail: m.arrigoni@fkf.mpg.de; s.weiglein@fkf.mpg.de

E.A. Kotomin
Max Planck Institute for Solid State Research, Heisenbergstraße 1, 70569 Stuttgart, Germany

Institute for Solid State Physics, University of Latvia, Kengaraga 8, 1063 Riga, Latvia
e-mail: e.kotomin@fkf.mpg.de

W.E. Nagel et al. (eds.), *High Performance Computing in Science and Engineering '15*, DOI 10.1007/978-3-319-24633-8_12

respectively. Oxygen vacancies are common point defects in these materials and have been shown to influence a variety of properties, such as mechanical and optical [4, 5] as well as ionic conductivity [6].

$BaZrO_3$ is a cubic perovskite that has attracted considerable attention in recent years, it has been used as dielectric material for wireless communication devices, hybrid perovskite-polymer-magnetic nanocomposites and as a substrate for thin films. Additionally, Y-doped $BaZrO_3$ is a promising candidate material for protonic ceramic fuel cells operating in the range of 400–700 °C, due to its high solid state proton conductivity. Working at intermediate temperatures improves the devices durability and compatibility between components and is thus more favorable than operating at the usual temperature range of 800–1000 °C of ceramic solid oxides fuel cells. Other electrochemical applications of Y-doped $BaZrO_3$ entails sensors and hydrogen pumps fabrication. The proton conductivity arises from incorporation of protons in the doped material by a dissociative absorption of water molecules upon exposure to humid atmospheres. Thus, fully charged oxygen vacancies play here a crucial role. Although charged vacancies dominate acceptor doped oxides, vacancies with two trapped electrons (the color F centers) are more common in undoped oxides under reducing conditions where the electron chemical potential is higher. These two charge states of the oxygen vacancies represent the limiting cases in partly ionic and covalent perovskites, where electrons are neither fully localized in the oxygen vacancy by electrostatic fields, as in more ionic compounds like MgO, nor are completely localized on the dangling bonds of the nearest cations, as in more covalent materials such as silicates.

Density functional approaches have in the recent decade been proved to be an important tool in defect analyses of functional oxides, and are now routinely applied in investigations of the electronic properties and defects thermodynamics. The majority of such investigations, however, consider the thermodynamic properties of defects only at 0 K, while most physical and chemical processes occur at moderate or high temperatures.

An important contribution to the thermodynamic properties at finite temperatures is given by the vibrational partition function, which can be evaluated by calculating the material's normal modes of lattice vibrations. There are still few reports on $BaZrO_3$. Sundell et al. [7] addressed defect entropies in $BaZrO_3$ from a computational perspective through the simplified Einstein model and considered only the vibrational contributions due to changes in the vibrational properties of the eight oxygen atoms nearest to the charged oxygen vacancy, thereby neglecting long range and volume relaxations effects.

Calculations of vibrational frequencies may also reveal structural instabilities through low frequency or imaginary phonon modes, allowing for identification of eventual soft modes responsible for phase transitions. According to experimental X-ray and neutron powder diffraction analyses, $BaZrO_3$ does not undergo any phase transition down to 2 K [8]. First principles studies of $BaZrO_3$ with the LDA [8] and GGA [9] exchange-correlation functionals have, however, indicated structural instabilities at the R- and/or M-points of the Brillouin zone that would lead to an antiferrodistortive transition at low temperatures. This disagreement

with experiments has been suggested to stem from neglect of zero-point motions [8] and/or anharmonic effects [10], which could suppress the phase transition. On the other hand, the employment of the hybrid PBE0 functional has shown a significantly better agreement with the experimental frequencies at the Γ-point and the absence of imaginary modes at any of the high symmetry reciprocal space points [11]. These contradictory results illustrate the importance of suitable choice of computational approach when evaluating the vibrational properties of, especially, perovskite structured oxides.

In this study, we employed the linear combination of atomic orbitals (LCAO) approach with the hybrid HF-DFT PBE0 functional [12] for investigating of the structural, electronic and vibrational properties of oxygen vacancy defects in the two different charge states (0 or +2) in bulk $BaZrO_3$. Particular emphasis is given to the vibrational contributions on the defect thermodynamic properties.

2 Methods

The fundamental quantity determining the thermodynamic stability of a defect is its free energy of formation, which, for an isolated oxygen vacancies in charge state q, takes the form:

$$\Delta_f G_{(v_O,q)}(T) = G_{(v_O,q)}(T) - G_{perfect}(T) + \mu_O(T,p_i) + q\mu_e, \tag{1}$$

where, $G_{(v_O,q)}(T)$ and $G_{perfect}(T)$ are the Gibbs free energy of the defective and non-defective system respectively, while $\mu_O(T,p_i)$ and μ_e are the chemical potentials of oxygen and electrons. $\mu_O(T,p_i)$ is taken as half that of the O_2 molecule Gibbs energy:

$$\mu_O(T,p_i) = \frac{1}{2}G_{O_2}(T). \tag{2}$$

For electrons, μ_e may take values from the top of the valence band to the bottom of the conduction band. Equation (1) was firstly suggested in this form by Zhang and Northrup [13]. In the present study we generalized it including vibrational contributions.

As the main focus of this work is to determine the contribution from phonons to the Gibbs free energy of defect formation, it is convenient to separate $\Delta_f G_{(v_O,q)}(T)$ into electronic, vibrational and gas phase contributions:

$$\begin{aligned}\Delta_f G_{(v_O,q)}(T) = \\ \Delta_f E^{el}_{(v_O,q)}(T) + \Delta_f H^{vib}_{(v_O,q)}(T) - T\Delta_f S^{vib}_{(v_O,q)}(T) + \mu_O(T,p_i) + q\mu_e,\end{aligned} \tag{3}$$

where Δ quantities are the differences between the defective and non-defective systems given property (H, S, ecc.). $\Delta_f H^{vib}$ and $\Delta_f S^{vib}$ are determined from the calculated harmonic vibrational frequencies ($\nu_s(\mathbf{q}), s = 1,2,\ldots,3N$, where N is

the number of atoms in the unit cell and **q** is a reciprocal lattice vector in the first Brillouin zone) according to:

$$G^{vib}(T) = \sum_{s,\mathbf{q}} \left(n_{s,\mathbf{q}}(T) + \frac{1}{2} \right) h\nu_s(\mathbf{q}) \\ -T \sum_{s,\mathbf{q}} \left(\frac{n_{s,\mathbf{q}}(T)}{T}) h\nu_s(\mathbf{q}) - k_B ln \left(1 - e^{-\frac{h\nu_s(\mathbf{q}}{k_B T}} \right) \right) + pV, \tag{4}$$

where the first sum represent the vibrational internal energy U^{vib} (zero point energy included) and the second one the vibrational entropy, S^{vib}. $n_{s,\mathbf{q}}(T)$ is the Bose-Einstein distribution $\left(e^{\frac{h\nu_s(\mathbf{q})}{k_B T}} - 1 \right)^{-1}$ and pV is the product between the system pressure and volume.

2.1 Computational Details

The calculations were performed employing localized basis sets (LCAO) and the hybrid HF-DFT Perdew-Burke-Ernzerhof exchange-correlation functional (PBE0) as implemented in the CRYSTAL14 code [14, 15].

The employed atomic basis sets (BSs) consisted of Gaussian-type functions and pseudopotentials. The basis set included quasi-relativistic pseudopotentials taken from the pseudopotential library of Stuttgart-Cologne group (http://www.theochem.uni-stuttgart.de/pseudopotentials/clickpse.html) for 46 core electrons of Ba and 28 core electrons of Zr. In order to avoid spurious interactions between the diffuse functions and the core functions of neighboring atoms, the basis set diffuse exponents smaller than 0.1 bohr^{-2} were removed as well as f-electron virtual functions. The all-electron BS 8-411G was used for O atoms. The tolerance factors of 7,7,7,7 and 14 for the Coulomb and exchange integrals were used. For all the studied defects we considered only the closed shell electronic configuration and setting the SCF calculations threshold value for energy convergence to 10^{-7} eV.

The neutral oxygen vacancy was modeled by removing a single O atom, keeping the BS of the vacant oxygen atom by means of a spurious 'ghosts' atom with no atomic mass. The latter approach allows for localization of electrons within the vacancy itself. The charged oxygen vacancy was modeled by removing two electrons from the overall supercell through charge compensation by a homogeneous jellium background charge. The energetics of these removed electrons is taken into account in the expression of the defect formation energy through the electron chemical potential (Eqs. (1) and (3)); while they do not given any contribution to $G^{vib}(T)$ (Eq. (4)), which entails only the vibrational degrees of freedom of the ions. Calculations were performed with 2×2×2 (40 atoms) and 3×3×3 (135 atoms) supercell expansions of the 5-atoms primitive cubic cell of $BaZrO_3$, corresponding to defect concentrations of 12.5 and 3.7 % respectively. Electronic integration over the Brillouin zone was performed using a 8×8×8 Monkhorst-Pack [16] k-mesh for

the five atoms unit cell. For supercell expansions, the k-mesh density was reduced accordingly.

Vibrational frequencies were calculated within the harmonic approximation by numerical evaluation of the dynamical hessian matrix elements through the first derivative of the atomic energy gradients, displacing each atom along the Cartesian coordinates by 0.001 Å.

2.2 Computational Resources

Supercell calculations deal with a relatively large amount of atoms. In this study we employed 2×2×2 and 3×3×3 supercells, formed by 40 and 135 atoms respectively. The presence of defects reduce the crystal symmetry, drastically increasing the computational costs. Approximately, each geometry optimization calculation of defective $BaZrO_3$ required 20 nodes and 24 h using the smallest supercell and up to 32 nodes and 96 h with the largest one for each run. Phonons calculations are much more demanding and required at least 20 nodes and up to two weeks per single run. On average 500.000 core-hours per month were approximately used. All calculations were performed on HLRS CRAY XE6 supercomputer at Stuttgart University.

3 Results and Discussion

3.1 Defective-Free Barium Zirconate

Table 1 compares various bulk properties of $BaZrO_3$ calculated in this work with the PBE0 functional with selected literature reports. The lattice parameter is in very good agreement with the experimental value of 4.192 Å[17]. The pure

Table 1 Lattice parameter (a), various bonding lengths (d), Mulliken atomic charges in LCAO calculations (q) and band gap ΔE_g

	LCAO				PW	
	PBE0[a]	PBE [9]	PBE0 [11]	B3LYP [19]	PW91 [9]	Expt.
a, Å	4.195	4.242	4.198	4.234	4.207	4.192 [17]
d(Zr-O), Å	2.098					
d(Ba-O), Å	2.966					
d(O-O), Å	2.966					
q(Ba), *e*	1.66		1.87	1.81		
q(Zr), *e*	2.35		2.21	2.15		
q(O), *e*	−1.33		−1.36	−1.32		
ΔE_g, eV	5.36		5.4	4.79		5.33 [18]

[a] Current study

The values are compared with those found in the literature from different computational studies and experiments

DFT functionals predict larger lattice parameter than the hybrid PBE0 functional, except for the study [9] where the PW91 was applied. The PBE0 functional yields an indirect band gap (M→ Γ) of 5.36 eV, being in very good agreement with the experimental value of 5.33 eV [18]; whereas the hybrid B3LYP functional noticeably underestimates it [19]. Correct evaluation of the optical band gap is crucial when evaluating the occupied donor state of the neutral oxygen vacancy. As is common, pure DFT functionals heavily underestimate this gap.

Mulliken atomic charges calculations reveal non-integer atomic charges for all elements, reflecting the partial ionic character of $BaZrO_3$. Moreover, the calculations show an overlap population charge of 68 me for the Zr-O bond, and almost zero for Ba-O, indicative of larger covalent character of the former bond.

Table 2 reports the vibrational frequencies at the Γ-point calculated in this study, including the splitting between transverse and longitudinal optical modes (T.O.-L.O. splitting), and their experimental values [20]. Due to the cubic symmetry of $BaZrO_3$ (space group O_h^1 number 221), one obtains the following set of optical phonon modes at the Γ-point: $4t_{1u} + t_{2u}$. The obtained results are in good agreement with the experimental values. The Zr-O_3 torsion mode is both IR and Raman inactive (silent mode of t_{2u} symmetry) and cannot be detected experimentally. In particular, due to the cubic symmetry, there are no Raman allowed vibrational modes in $BaZrO_3$ and thus the L.O. frequencies are not detectable from experiments. Although the T.O.-L.O. splitting is very pronounced, we found that its contribution to the thermodynamic potentials is negligible (taking it into account, G^{vib} increases at maximum 0.1 eV in the range 0–1600 K), and was thus not accounted for in the defective calculations. To further investigate the vibrational properties and structural stability of $BaZrO_3$, we calculated the phonon dispersion relation along the $\Gamma \rightarrow X \rightarrow M \rightarrow \Gamma \rightarrow R \rightarrow M \rightarrow \Gamma$ path in the BZ. The curves shown in Fig. 1 were obtained by interpolating the discrete points obtained with a 2×2×2 supercell. The frequencies obtained by us are in agreement with those reported by Evarestov [11] employing the same code and functional. No imaginary modes where observed, therefore we predict a stable cubic structure for $BaZrO_3$.

Table 2 Calculated and experimental vibrational translational optic frequencies at the Γ-point for defective-free $BaZrO_3$. We have also reported the split of the longitudinal optics modes

	Calculated		Expt.[21]
Mode, cm^{-1}	T.O.	L.O.	T.O.
Ba-ZrO_3 stretch	125	145	115
O-Zr-O bend	219	406	210
Zr-O_3 torsion	220	–	Inactive
Zr-O stretch	511	718	505

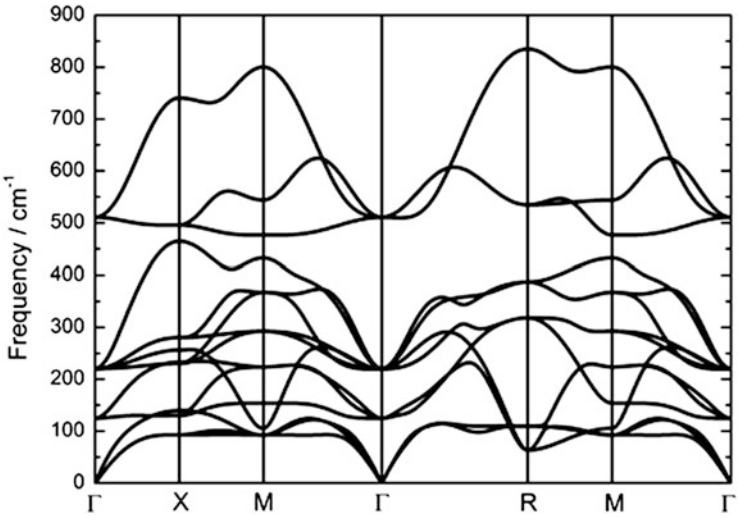

Fig. 1 Vibrational band structure for $BaZrO_3$ calculated with CRYSTAL in this study. The **q**-points sample was formed by the Γ-, M-, X- and R-points. Continuous curves were obtained using a Fourier interpolation technique

3.2 Oxygen Vacancies: Atomic and Electronic Properties

Table 3 shows structural relaxation induced by the neutral and charged oxygen vacancies in $BaZrO_3$ using 2×2×2 and 3×3×3 supercell expansions. The neutral vacancy leads to a slight contraction of the cell for both defect concentrations. We suggest this effect to be related to the inclusion of the 'ghost' basis functions in the vacancy that, in order to decrease the energy of the defect-induced level (the position of defect-induced level on the band structure, Fig. 2), yields to the c-axis shrinks to maximize the overlap between the 'ghost' orbitals and the *p*, *d* orbitals of the nearest Zr atoms. We in addition performed a test calculation leaving vacuum (i.e no 'ghost' basis functions) in the neutral oxygen vacancy and noticed that the c-axis, and in particular the distances between Zr atoms in the Zr-v_O-Zr complex, expands; while the other two axes shrink. A comparison of our results for the two cases, i.e. with ghost functions and leaving vacuum in the vacancy position, revealed lower formation energy of oxygen vacancy for the former .

Our study shows the new band induced by $v_O^{\times}$ defect is fully occupied (see Fig. 2), with its maximum occurring at the M-point of the first BZ and situated below the conduction band. The band is located deep in the band gap, with a minimum distance to the conduction band minimum of 1.31 eV (1.58 eV in the 3×3×3 supercell), in agreement with previous reports of deep F-center induced defect levels in zirconate perovskites modelled with a 'ghost' BS [22]. The F-center partly reduces the two nearest Zr atoms, as the two electrons in the defective level are mostly localized on their *d*-states (Fig. 2).

Table 3 Relative lattice constant ($\Delta a/a_0$, $\Delta b/b_0$, $\Delta c/c_0$) relaxations, formation volume ($\Delta_f V$), relative volume relaxation ($\Delta V/V_0$), minimum distance between the conduction band minimum and defective level ($\Delta\epsilon$) and defective band width ($\delta\epsilon$) of the oxygen vacancy in the charge state 0 ($v_O^{\times}$) and +2 ($v_O^{\bullet\bullet}$), calculated using 2×2×2 (8 f.u.) and 3×3×3 supercell expansion (27 f.u.)

Expansion	2×2×2		3×3×3	
Defect	$v_O^{\times}$	$v_O^{\bullet\bullet}$	$v_O^{\times}$	$v_O^{\bullet\bullet}$
$\Delta a/a_0$ (%)	−0.29	−13.4	0.08	−12.7
$\Delta b/b_0$ (%)	−0.29	−13.4	0.08	−12.7
$\Delta c/c_0$ (%)	−0.88	−10.6	−0.66	−10.7
$\Delta_f V$ (Å^3)	−1.07	−27.1	−0.37	−26.6
$\Delta V/V_0$ (%)	−1.45	−37.3	−0.50	−36.3
$\Delta\epsilon$ (eV)	1.31	0.20	1.58	0.20
$\delta\epsilon$ (eV)	0.78	0.74	0.15	0.13

The relative relaxations are given as percentile relative expansion per mole fraction of oxygen vacancies. The formation volume is defined as the difference between the defective and defective-free supercell volumes. In accordance with local site symmetry of oxygens (point group symmetry D_{4h}) in cubic perovskite BaZrO3, the symmetry of defective supercells lowers to space group D_{4h}^1

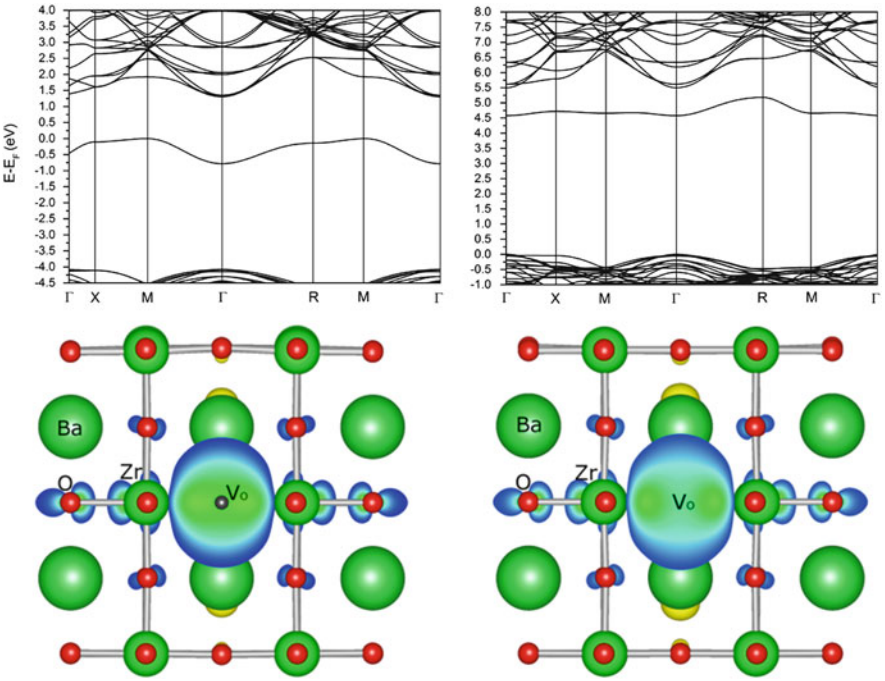

Fig. 2 *Top*: Band structure of the 2×2×2 $BaZrO_3$ supercell with a $v_O^{\times}$ (*left*) and $v_O^{\bullet\bullet}$ (*right*) oxygen vacancy. *Bottom*: electronic charge density projected on the defective level obtained modelling the vacancy using the ghost BS (*left*) or leaving vacuum (*right*). The isosurface threshold level is set to 0.002 e/a_0^3; points with an electron charge density value greater than the threshold lies inside the isosurface (the larger the value the warmer the color)

For the charged vacancy, Mulliken charge analyses indicated a small charge of merely 0.2 *e* associated with the vacancy ghost BS; hence the site is effectively positively charged and repels the nearest Zr and Ba cations while it attracts the nearest oxide anions. This is clearly shown in Table 3. In particular, $v_O^{\bullet\bullet}$ induces a large outward displacement of the two nearest Zr ions, resulting in an anisotropic relaxation that yields a tetragonal defective cell. The inward relaxation of the eight nearest O ions is significantly larger for $v_O^{\bullet\bullet}$ than $v_O^{\times}$, resulting in a general contraction in all directions, and thus a large negative formation volume. Finally, the anisotropic relaxations induced by the oxygen vacancies reduce the symmetry of defective supercells to space group D_{4h}^1 (123). For the charged vacancy, the defective induced band is unoccupied and lies much closer to the conduction band bottom with respect to the neutral defect (only 0.20 eV for both supercell sizes).

3.3 *Oxygen Vacancies: Thermodynamic Properties*

Figure 3 shows the vibrational density of states (DOS) for $v_O^{\times}$ and $v_O^{\bullet\bullet}$ calculated with the 2×2×2 and 3×3×3 supercells. Both defects induce a distinguishable vibrational peak at around 660 cm^{-1} in the 2×2×2 supercell, and 676 and 630 cm^{-1} in 3 × 3 × 3 supercell for $v_O^{\times}$ and $v_O^{\bullet\bullet}$, respectively, originating from Zr-O stretch relative to the two Zr atoms closest to the vacancy. This mode belongs to the A_1 irreducible representation of the space group and is thus both IR and Raman active. Its IR intensity, evaluated through the Berry phase approach, values 446 km/mol (2×2×2 supercell) and 464 km/mol (3×3×3 supercell) for $v_O^{\times}$, and around 704 km/mol (2×2×2 supercell) and 1394 km/mol (3×3×3 supercell) for $v_O^{\bullet\bullet}$, and should therefore be detectable in experiments. These results agree with those of a previous study on $SrTiO_3$ [23] that shown a vibrational mode at around 630 cm^{-1} appearing

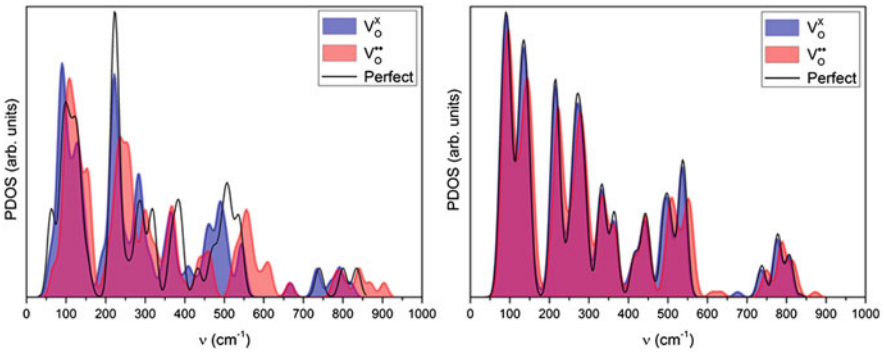

Fig. 3 Phonon density of states (PDOS) calculated for the 2×2×2 (*left*) and 3×3×3 (*right*) BaZrO3 supercells. In each plot the PDOS is reported for the perfect system (*unfilled curve*) and the defective systems containing the neutral oxygen vacancy $v_O^{\times}$ (*blue*) and the double charged oxygen vacancy $v_O^{\bullet\bullet}$ (*red*)

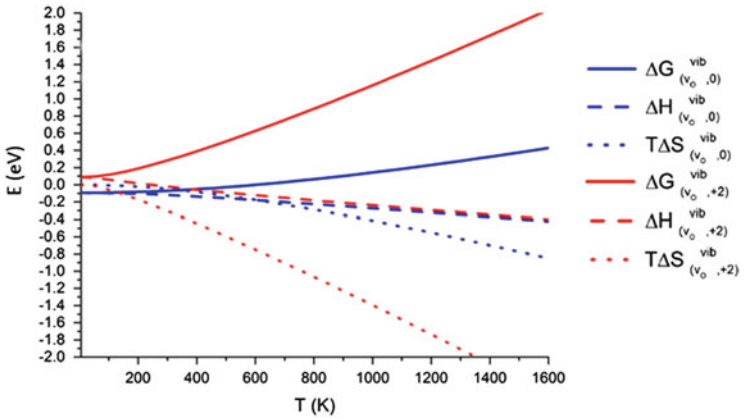

Fig. 4 Phonon contribution to the formation enthalpy, entropy and Gibbs free energy (cfr. Eq. (3)) for neutral and charged oxygen vacancies, calculated with a 3×3×3 supercell

in presence of neutral oxygen vacancies and corresponding to the relative motion of Ti and O atoms near the vacancy. In addition, the large negative formation volume of $v_O^{\bullet\bullet}$ leads to stiffening of the bonds and thus a general blue-shift of all vibrational frequencies.

Figure 4 shows the corresponding phonon contribution to the formation enthalpy, entropy and Gibbs free energy of $v_O^{\times}$ and $v_O^{\bullet\bullet}$ calculated using both 2×2×2 and 3×3×3 supercells. At T=0 K the only contribution to ΔG^{vib} is the difference in zero-point energy between the defective and perfect supercells. For $v_O^{\times}$, $\Delta H^{vib} < 0$ at 0 K with both supercells, as expected due to the removal of three vibrational degrees of freedom upon vacancy formation. For $v_O^{\bullet\bullet}$, however, $\Delta H^{vib} > 0$ at 0 K, which stems from the blue-shift of the phonon spectrum due to the considerable negative formation volume. Further, ΔH^{vib} decreases with increasing temperature for both defects, reflecting a negative contribution from phonons to the formation enthalpy. The larger blue shift of the vibrational frequencies in the 2×2×2 than in the 3×3×3 supercell, Fig. 4, slightly increases the enthalpy of the defective system. The shift is even more pronounced for $v_O^{\bullet\bullet}$ and therefore $\Delta H^{vib}_{(v_O,+2)}$ (0 K) is around 0.08 eV larger in the smaller supercell than in the larger; while for $v_O^{\times}$ the difference in $\Delta H^{vib}_{(v_O,0)}(0\,K)$ is around 0.03 eV only.

The calculated $\Delta_f S^{vib}$ is negative for both $v_O^{\times}$ and $v_O^{\bullet\bullet}$. $\Delta_f S^{vib}$ is not affected by the supercell size and its value is modest within the considered temperature range, as expected from the negligible effect of $v_O^{\times}$ on the PDOS. On the other hand, $\Delta_f S^{vib}$ is significantly larger (more negative) with the 3×3×3 than the 2×2×2 supercell, due to the larger number of vibrational modes and the wider local structural relaxation allowed by the former supercell.

The calculated $\Delta_f S^{vib}$ is considerably more negative for $v_O^{\bullet\bullet}$ than $v_O^{\times}$, as expected from both the greater local relaxations, and the more negative formation volume of the former. Therefore, the vibrational contribution to the Gibbs free energy

($\Delta_f G^{vib}$) of formation is particularly relevant for $v_O^{\bullet\bullet}$ and at high temperature. This is illustrated in Fig. 4, which shows $\Delta_f G^{vib}$ of $v_O^{\bullet\bullet}$ and $v_O^{\times}$ calculated with a 3×3×3 supercell at standard pressure.

4 Conclusions

In this contribution we performed first principles calculations to determine the electronic and thermodynamic properties of oxygen vacancies in $BaZrO_3$ with emphasis on the contribution from phonons. We employ LCAO calculations using the CRYSTAL14 code and the hybrid PBE0 functional. For defective-free $BaZrO_3$, we predicted a cell parameter, optical band gap and vibrational frequencies at the Γ-point in very good agreement with the experiments.

We find that $v_O^{\times}$ creates a deep level in the band gap (around 1.5 eV from the conduction band bottom), while $v_O^{\bullet\bullet}$ a shallower one at 0.2 eV from the conduction band bottom. Both vacancy charge states induce a new IR and Raman active lattice vibration at around 650 cm^{-1} that, according to this study, could be experimentally detectable. These results agree with recent observations in defective $SrTiO_3$ [23] and could therefore be a general feature of oxygen vacancies in perovskite-structured oxides. The charged oxygen vacancy, $v_O^{\bullet\bullet}$, induces significantly larger structural distortions than the neutral one, $v_O^{\times}$, which causes a noticeable blue shift of the vibrational spectrum. Hence, while the contribution from phonons the Gibbs free energy of formation of $v_O^{\times}$ is small, phonons increase that of $v_O^{\bullet\bullet}$ by circa 1 eV at 1000 K (under standard pressures).

Acknowledgements Authors greatly appreciated help and support from the High Performance Computer Center in Stuttgart (HLRS, project DEFTD 12939).

References

1. Walsch, A., Sokol, A., Catlow, C.R.A.: Energy storage: rechargeable lithium batteries. In: Computational Approaches to Energy Materials. Wiley, New York (2013)
2. Kuklja, M.M., Kotomin, E.A., Merkle, R., Mastrikov, Yu.A., Maier, J.: Combined theoretical and experimental analysis of processes determining cathode performance in solid oxide fuel cells. Phys. Chem. Chem. Phys. **15**, 5443–5471 (2013)
3. Donnerberg, H.J.: Atomic Simulations of Electro-Optical and Magneto-Optical Materials. Springer Tracts in Modern Physics. Springer, Berlin (1999)
4. Scott, J.F., Dawber, M.: Oxygen-vacancy ordering as a fatigue mechanism in perovskite ferroelectrics. App. Phys. Lett. **76**, 3801–3803 (2000)
5. Hwang, H.Y.: Perovskites: oxygen vacancies shine blue. Nat. Mater. **4**, 803–804 (2005)
6. Merkle, R., Maier, J.: How is oxygen incorporated into oxides? A comprehensive kinetic study of a simple solid-state reaction with $SrTiO_3$ as a model material. Angew. Chem. Int. Ed. **47**, 3874–3894 (2008)

7. Sundell, P.G., Björketun, M.E., Wahnström, G.: Thermodynamics of doping and vacancy formation in $BaZrO_3$ perovskite oxide from density functional calculations. Phys. Rev. B **73**, 104112 (2006)
8. Akbarzadeh, A.R., Kornev, I., Malibert, C., Bellaiche, L., Kiat, J.M.: Combined theoretical and experimental study of the low-temperature properties of $BaZrO_3$. Phys. Rev. B **72**, 205104 (2005)
9. Bilić, A., Gale, J.D.: Gale: Ground state structure of $BaZrO_3$: a comparative first-principles study. Phys. Rev. B **79**, 174107 (2009)
10. Magyari-Köpe, B., Vitos, L., Grimvall, G., Johansson, B., Kollár, J.: Low-temperature crystal structure of $CaSiO_3$ perovskite: an *ab initio* total energy study. Phys. Rev. B **65**, 193107 (2002)
11. Evarestov, R.A.: Hybrid density functional theory LCAO calculations on phonons in $Ba(Ti,Zr,Hf)_3$. Phys. Rev. B **83**, 014105 (2011)
12. Perdew, J.P., Ernzerhof, M., Burke, K.: Generalized gradient approximation made simple. J. Chem. Phys. **105**, 9982–9985 (1996)
13. Zhang, S.B., Northrup, J.E.: Chemical potential dependence of defect formation energies in GaAs: application to Ga self-diffusion. Phys. Rev. Lett. **67**, 2339–2342 (1991)
14. Dovesi, R., Saunders, V.R., Roetti, R.O.C., Zicovich-Wilson, C.M., Pascale, F., Civalleri, B., Doll, K., Harrison, N.M., Bush, I.J., D'Arco, P., Llunell, M., Causà, M., Noël, Y.: CRYSTAL14 User's Manual University of Torino, Torino (2014)
15. Dovesi, R., Orlando, R., Erba, A., Zicovich-Wilson, C.M., Civalleri, B., Casassa, S., Maschio, L., Ferrabone, M., De La Pierre, M., D'Arco, P., Noël, Y., Causà, M., Rérat, M., Kirtman, B.: CRYSTAL14: a program for the ab initio investigation of crystalline solids. Int. J. Quant. Chem. **114**, 1287–1317 (2014)
16. Monkhorst, H.J., Pack, J.D: Special points for Brillouin-zone integrations. Phys. Rev. B **13**, 5188–5192 (1976)
17. Pies, W., Weiss, A.: *Landolt–Börnstein.* Numerical data and functional relationships in science and technology, Group III. In: Crystal and Solid State Physics, Vol. 7. Crystal Structure Data of Inorganic Compounds. Parts a and g. A. Acta Cryst. A. International Union of Crystallography (1975)
18. Robertson, J.: Band offsets of wide-band-gap oxides and implications for future electronic devices. J. Vac. Sci. Technol. B **18**, 1785–1791 (2000)
19. Eglitis, R.I.: Ab initio calculations of the atomic and electronic structure of $BaZrO_3$ (111) surfaces. Solid State Ionics **230**, 43–47 (2013)
20. Parida, S., Rout, S.K., Cavalcante, L.S., Sinha, E., Li, M.S., Subramanian, V., Gupta, N., Gupta, V.R., Varela, J.A., Longo, E.: Structural refinement, optical and microwave dielectric properties of $BaZrO_3$. Ceram. Int. **38**, 2129–2138 (2012)
21. Perry, C.H., McCarthy, D.J., Rupprecht, G.: Dielectric dispersion of some perovskite zirconates. Phys. Rev. **138**, A1537–A1538 (1965)
22. Zhukovskii, Y.F., Kotomin, E.A., Piskunov, S., Ellis, D.E.: A comparative ab initio study of bulk and surface oxygen vacancies in $PbTiO_3$, $PbZrO_3$ and $SrTiO_3$ perovskites. Solid State Commun. **149**, 1359–1362 (2009)
23. Evarestov, R., Blokhin, E., Gryaznov, D., Kotomin, E.A., Merkle, R., Maier, J.: Jahn-Teller effect in the phonon properties of defective $SrTiO_3$ from first principles. Phys. Rev. B, **85**, 174303 (2012)